APPLIED ORGANOMETALLIC CHEMISTRY, VOL. 10, 283–295 (1996)

Theoretical Studies of Simple Organoboron Compounds: Structures and Stabilities of BC_2H_4 Isomers

Antonio Largo* and Carmen Barrientos*
Departamento de Química Física y Analítica, Facultad de Química, Universidad de Oviedo, 33006 Oviedo, Spain

An *ab initio* study of the BC_2H_4 has been carried out. Several isomers have been studied: boron–ethylene complexes resulting from perpendicular and σ interactions, boron–methylcarbene type structures, open and cyclic insertion products with a B–H bond, and isomers with two B–H bonds. Geometries at the second-order Møller–Plesset level have been obtained for ten species, and their characteristics have been tested through computation of vibrational frequencies. Special attention has been paid to their molecular structure, trying to rationalize the bonding in these species, particularly in the case of cyclic isomers. Electronic energies have been computed at the fourth-order Møller–Plesset level. Our theoretical calculations predict that the global minimum is the H_2BCCH_2 isomer ($^2B_2$ electronic state), with the HBH plane perpendicular to the CCH_2 moiety, and that it lies about 66 kcal mol^{-1} (276 kJ mol^{-1}) below ground-state boron+ethylene. Nevertheless there are other isomers which are also quite stable and might be accessible to experimental detection, such as $HBCHCH_2$ and H_2BCHCH (both with $^2A'$ electronic states) which lie 8 (33.5) and 13 kcal mol^{-1} (54.4 kJ mol^{-1}), respectively, above the global minimum, as well as two cyclic structures, the insertion product $HBC_2H_3(^2A'')$ and the boron–ethylene π-complex BC_2H_4 ($^2A_1$), which are relatively stable since they lie 12 (50) and 22 kcal mol^{-1} (92 kJ mol^{-1}), respectively, higher than H_2BCCH_2.

Keywords: boron; carborane; structure; theoretical studies; electronic energy; isomers

1 INTRODUCTION

Nowadays quantum chemistry can be applied to a wide variety of systems, ranging from small molecules to very complex ones. This is feasible not only because of the outstanding advances in theory but also because of the dramatic revolution in computers in recent years. Nevertheless this optimism should be viewed realistically since it is clear that the degree of accuracy one can achieve depends very much on the size of the system under study. This is especially important when interest is focused on the development of new materials. A well-known example is the study of the linear and nonlinear optical properties of new materials (which in the case of organoboron compounds is addressed by Marder elsewhere in this issue[1]). Undoubtedly quantum chemistry can help in this field by rationalizing experimental results and, most importantly, predicting polarizabilities and hyperpolarizabilities prior to experiment, and therefore guiding the preparation of new materials. However, it must be recognized that calculations of second hyperpolarizability coefficients are only reliable for rather small systems. Therefore the usual approach is to carry out theoretical studies on small systems which are used as models for more complex cases, often allowing extrapolation of different properties.

In a similar way the interactions of atoms and small molecules have been a very important research area for both theoretical and experimental studies.[2,3] For these small systems high-level computational methods can be applied and therefore predictions and/or interpretation of experimental facts can be made on a solid basis. But

* New address, from October 1995: Departamento de Química Física, Facultad de Ciencias, Universidad de Vallodolid, 47005 Valladolid, Spain.

CCC 0268–2605/96/030283–13

Received 15 April 1995
Accepted 9 June 1995

there is another reason for the interest in this area: a good knowledge of the interactions in simple systems is essential to understand the behaviour of more complex ones.

Until recently the study of aluminium–hydrocarbon compounds has received much more attention than that of their boron counterparts. Several aluminium adducts have been observed employing different techniques—mainly ESR, IR or UV spectroscopy. For example we can mention the work on compounds such as $AlCH_4$,[4] AlC_2H_2,[5–7] AlC_2H_4[6–11] and $Al(C_2H_4)_2$.[12] From the theoretical side, several studies have also addressed the structures and stabilities of these species, particularly in the case of AlC_2H_2,[13–18] AlC_2H_4[13,15,17,19] or simple aluminium–carbon clusters such as AlC_2,[20] Al_2C or Al_2C_2.[21]

Nevertheless, boron atom chemistry has recently received much attention, due to the possibility of using laser ablation for producing boron atoms. Reactions of boron atoms with small molecules produced new boron species which have been characterized (trapped in inert matrices) by ESR and IR spectroscopies.[22–34] Of particular relevance are the reactions of boron atoms with small hydrocarbons, which have also stimulated theoretical work in this field. A theoretical study[35] of the boron–methane reaction has shown that production of CH_3BH is exothermic by about 50 kcal mol^{-1}, (209 kJ mol^{-1}) although both dissociation into $CH_2BH + H$ and rearrangement to CH_2BH_2 are energetically favourable. The reaction of boron with acetylene is also interesting for different reasons. A proper understanding of the interactions of boron with acetylene is important in order to propose reasonable mechanisms for the chemistry of carboranes. In addition, theoretical studies[36] have shown that there is a competition between insertion of boron into a C–H bond and addition to the C–C bond. The combined experimental and theoretical work of Andrews and co-workers[29,30] allowed identification of both the HBCCH insertion product and the BC_2H_2 borirene radical. The latter species exhibits molecular properties suggesting a delocalized π-bonding like that found for borirene (HBC_2H_2) and substituted borirene species.[37–39]

In this paper we present a theoretical study of the possible isomers produced in the interaction between atomic boron and ethylene. We hope that such a study may stimulate experimental work on this reaction, but may also give some insight into the nature of the bonding in boron–hydrocarbon compounds.

2 THEORETICAL METHODS

The geometries of the different BC_2H_4 isomers have been optimized using second-order Møller–Plesset (MP2) perturbation theory with the 6-31G** basis set.[40,41] This basis, set includes a set of polarization *p* functions on hydrogen and a set of *d* functions for boron and carbon. Harmonic vibrational frequencies were analyticaly computed at the MP2/6-31G* level and the zero-point vibrational energies (ZPVE) were included in the calculation of relative energies.

On the MP2/6-31G** optimized geometries, energy calculations at the fourth-order Møller–Plesset (MP4) level (including triple substitutions)[42,43] were carried out. In these calculations we employed the 6-311G** basis set[44] and assumed the 'frozen core' approximation (inner-shell molecular orbitals are not included for computing correlation energies). Since we will be dealing with open-shell states we will also provide projected fourth-order Møller–Plesset[45,46] values (PMP4), which are more reliable when spin contamination is observed (the S^2 expectation value for the Hartree–Fock reference function being different from the theoretical exact value, 0.75 for doublet states). All these calculations were carried out with the GAUSSIAN 92 *ab initio* program package.[47] A complete account on the *ab initio* methods employed in this work can be found in reference 48.

In the case of cyclic isomers the nature of bonding was characterized using Bader's topological analysis.[49] The one-electron density $\rho(r)$ was analysed through its gradient vector field $\nabla\rho(r)$, characterizing 'bond critical points' (a bond critical point is a minimum of $\rho(r)$ along the line linking nuclei and a maximum along the interatomic surfaces) and 'ring critical points' (corresponding to maxima in one direction and minima in two directions). In addition the Laplacian of $\rho(r)$ provides information on where the electronic charge is concentrated ($\nabla^2\rho(r) < 0$) or depleted ($\nabla^2\rho(r) > 0$). By employing the Laplacian of the electron density, the problem in defining a reference density in order to determine the difference density distribution (which informs on where the electron density is concentrated or depleted in a molecule) is avoided. The analysis of the charge density was performed with the AIMPAC[50] series of programs, and the MP2/6-311G** wavefunction was employed to compute the electron density.

3 RESULTS AND DISCUSSION

We have studied several conformations for the BC_2H_4 system that will be described in the following order: boron–ethylene complexes and ring structures (resulting from the perpendicular or σ approach of boron to the ethylene molecule); boron–methylcarbene structures corresponding to the connectivity $BCHCH_3$; open and cyclic insertion products with a B–H bond, and finally isomers with two B–H bonds of the types H_2BCHCH and H_2BCCH_2. The nature of stationary points on the (BC_2H_4) potential surface has been tested through computation of vibrational frequencies (a true minimum is characterized by having all frequencies real at a particular level of theory, whereas those structures which are shown to have one imaginary frequency correspond in fact to transition states at that level).

3.1 Boron–ethylene complexes and ring structures

The perpendicular approach of boron to C_2H_4 imposes C_{2v} symmetry on the system. Therefore the electronic configuration of ground-state ethylene (^1A_g electronic state in D_{2h} symmetry) becomes, under C_{2v} symmetry,

$C_2H_4(^1A_g, {}^1A_1)$:

$$(1a_1)^2(1b_2)^2(2a_1)^2(2b_2)^2(1b_1)^2(3a_1)^2(1a_2)^2(4a_1)^2 \quad (1)$$

For ground-state boron atoms (^2P) the triple degeneracy is lost under C_{2v} symmetry, resolving in $^2A_1$, $^2B_2$ and $^2B_1$ states:

$$B(^2P, {}^2A_1): (1a_1)^2 (2a_1)^2 (3a_1)^1 \quad (2)$$

$$B(^2P, {}^2B_2): (1a_1)^2 (2a_1)^2 (1b_2)^1 \quad (3)$$

$$B(^2P, {}^2B_1): (1a_1)^2 (2a_1)^2 (1b_1)^1 \quad (4)$$

Therefore three different electronic states can be obtained from combination with ethylene, with the following electronic configurations

$BC_2H_4(^2A_1)$:
{core}
$$(3a_1)^2 (2b_2)^2 (4a_1)^2 (1b_1)^2 (1a_2)^2 (5a_1)^2 (6a_1)^2 (7a_1)^1 \quad (5)$$

$BC_2H_4(^2B_2)$:
{core}
$$(3a_1)^2 (2b_2)^2 (4a_1)^2 (1b_1)^2 (1a_2)^2 (5a_1)^2 (6a_1)^2 (3b_2)^1 \quad (6)$$

$BC_2H_4(^2B_1)$:
{core}
$$(3a_1)^2 (2b_2)^2 (4a_1)^2 (ab_1)^2 (1a_2)^2 (5a_1)^2 (6a_1)^2 (2b_1)^1 \quad (7)$$

When one tries to obtain optimized structures for these electronic states it is found that only the $^2B_2$ and $^2B_1$ states are bound relative to $B + C_2H_4$, whereas the $^2A_1$ state is repulsive. Nevertheless for short $B–C_2H_4$ distances there is another $^2A_1$ state which lies below $B + C_2H_4$ and therefore represents a stable structure with the following electronic configuration

$BC_2H_4(^2A_1)$:
{core}
$$(3a_1)^2 (2b_2)^2 (4a_1)^2 (1b_1)^2 (1a_2)^2 (5a_1)^2 (3b_2)^2 (6a_1)^1 \quad (8)$$

It is obvious that this state does not correlate (in C_{2v} symmetry) with ground-state $B + C_2H_4$. Correlation can be established with either $B(^2P, {}^2B_2)$ + triplet ethylene or, alternatively, with excited boron (^2S, $^2A_1$) + ground-state ethylene.

The MP2/6-31G** optimized geometries for the $^2B_2$, $^2B_1$ and $^2A_1$ states, the latter corresponding to electronic configuration (8), are shown in Fig. 1. These structures will be referred to as **1**, **2** and **3**, respectively. The bonding in these structures can be understood in terms of the interactions between the valence orbitals of boron and ethylene. The basic ideas are already in the Dewar model and Chatt and Duncanson's σ-donation. π-backdonation model.[51–53] The interaction of the boron $2p_y$ orbital with the LUMO $\pi^*_{C=C}$ orbital of ethylene produces a b_2 orbital, whereas the $\pi_{C=C}$ orbital interacts with the $2p_z$ orbital of boron, as illustrated in Fig. 2. Therefore the repulsive nature of the $^2A_1$ state represented by electronic configuration (2) is easily understood, since it implies a three-electron interaction (the a_1 singly occupied orbital of $B(^2A_1)$ is precisely the $2p_z$ orbital). On the other hand the $^2B_2$ state comes from the interaction of a boron atom with an empty $2p_z$ orbital and one electron in the $2p_y$ orbital, which contributes to a favourable interaction. This $^2B_2$ state must be more stable

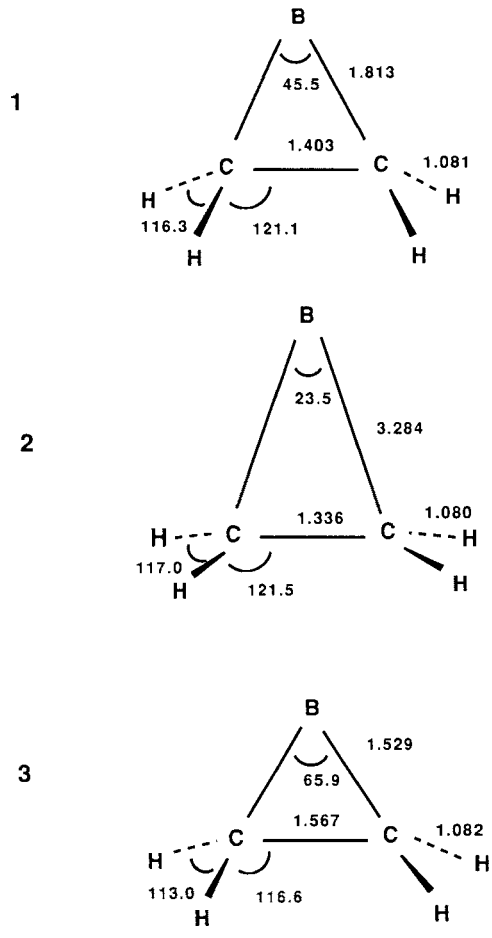

Figure 1 MP22/6-31G** optimized geometries for the C_{2v}-symmetry boron–ethylene complexes **1**–**3**. Bond distances are given in Å and angles in degrees.

than the $^2B_1$ state, where no b_2 interaction exists. The geometrical parameters of structures **1** and **2** (Fig. 1) are consistent with these ideas. The $^2B_1$ state exhibits a long B–C distance, with the C_2H_4 moiety preserving a geometry very close to that of ethylene, whereas the B–C bond is much shorter for the $^2B_2$ state (although it is still longer than typical B–C single bond lengths) and the C–C bond distance differs considerably from that of ethylene.

The situation is quite different for the $^2A_1$ state. Structure **3** shows geometrical parameters which correspond to two formal B–C bonds and a single C–C bond. A detailed analysis of electron configuration (8) reveals that, according to the previous considerations, the $5a_1$ orbital is essentially a $2p_z(B)$–$\pi_{C=C}$ molecular orbital and the $3b_2$ molecular orbital corresponds to the $2p_y(B)+\pi^*_{C=C}$ combination, whereas the $6a_1$ singly-occupied molecular orbital is basically a 2s(B) orbital. Therefore the valence bond structure shown in Fig. 3 can be assigned to **3** in full agreement with the geometry shown in Fig. 1. This view is also confirmed by a Mulliken population analysis which provides an atomic spin density of 0.92 for the boron atom, indicating that the unpaired electron is localized at B.

It is worth noting that the geometry of **3** is very similar to that found in HBC_2H_4.[54] In this study of three-membered rings the authors found that, as the electronegativity of the heteroatom bonded to ethylene increases, the C–C bond length decreases as a result of enhanced σ-bridged π-bonding [53] (the a_1 orbital in Fig. 2 contributes not only to side bonds but also to C–C bonding). In our case, B has a low electronegativity and therefore a long C–C bond distance should be expected. In fact, for a heteroatom like boron with smaller electronegativity than carbon, it should be expected that the b_2 orbital in Fig. 2 is

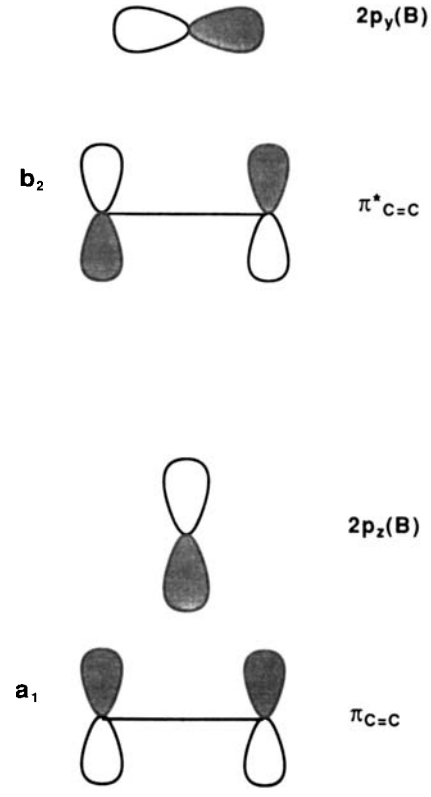

Figure 2 Interactions between the valence orbitals of boron and ethylene.

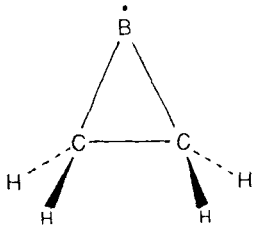

Figure 3 Valence bond structure of **3**.

more important thaN the a_1 orbital in building up the three-membered ring, since b_2 implies donation of electron charge from B to ethylene whereas the a_1 interaction corresponds to charge transfer from ethylene towards boron. That explains the very long distance for structure **2** (the b_2 orbital is empty and, in addition, the $5a_1$ molecular orbital has an almost negligible degree of participation for the boron atom), the intermediate bonding in structure **1** (one electron in b_2) and the bond distances in **3** (the b_2 orbital is fully occupied).

To obtain a deeper insight into the nature of bonding in these species, it is interesting to apply Bader's topological analysis of charge density.[49] The one-electron density distribution $\rho(r)$ is an appropriate magnitude since it is invariant under unitary transformations of molecular orbitals, and other molecular properties depend on it. This type of analysis has proved to be very useful in the study of three-membered rings.[55,56] We will employ for this analysis the gradient vector field of the one-electron density, $\nabla\rho(r)$, and its Laplacian $\nabla^2\rho(r)$. The importance of the gradient vector field of $\rho(r)$ resides in that it allows identification of critical points, which are the sources and sinks of the gradient paths of $\nabla\rho(r)$. The most interesting critical points in our context (apart from the nuclei which act as attractors since they correspond to maxima of electron density in three directions) are the so-called bond and ring critical points. Bond critical points are minima in one direction (between the two nuclei) and maxima along the other two directions. Therefore they have one positive and two negative eigenvalues of the Hessian of $\rho(r)$. On the other hand, ring critical points have one negative and two positive eigenvalues of the Hessian of $\rho(r)$, since they are minima in two directions. The presence or absence of a ring critical point implies the existence, or not, of a ring structure. The Laplacian of the electronic charge density, $\nabla^2\rho(r)$, provides information about the regions where electron density is concentrated ($\nabla^2\rho(r)<0$) and depleted ($\nabla^2\rho(r)>0$).

Gradient maps of the electronic charge density and contour maps of the Laplacian of $\rho(r)$ (in both cases on the plane defined by the boron and carbon atoms) for structures **1**, **2** and **3** are given in Figs 4, 5 and 6, respectively.

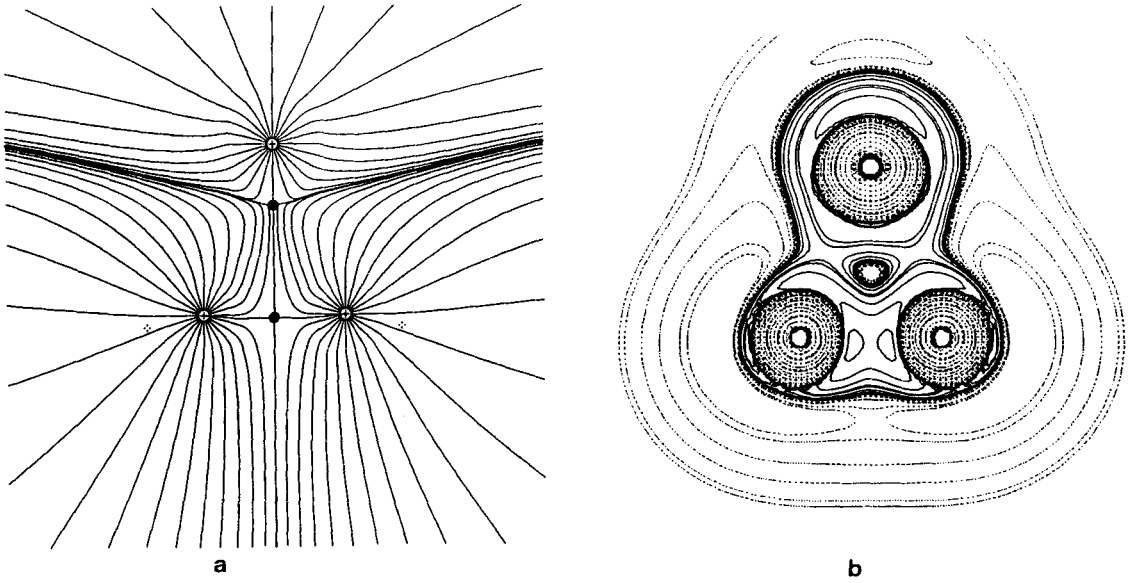

Figure 4 (a) Gradient map of the electronic charge density and (b) contour map of the Laplacian of $\rho(r)$, for structure **1** obtained at the MP2/6-311G** level. In (a) the nuclei are denoted by crosses and bond critical points by dots. In (b) negative values of $\nabla^2\rho(r)$ are denoted by solid contours and positive values by dotted contours. In both cases the CBC plane is considered.

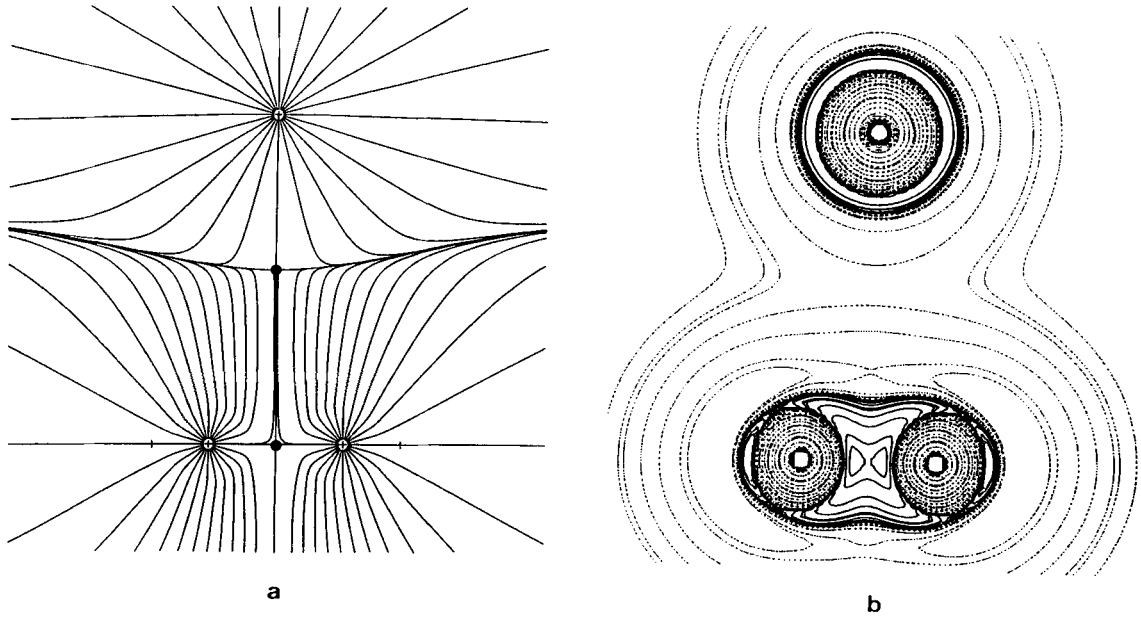

Figure 5 (a) Gradient map of the electronic charge density and (b) contour map of the Laplacian of $\rho(r)$, for structure **2** obtained at the MP2/6-311G** level. In (a) the nuclei are denoted by crosses and bond critical points by dots. In (b) negative values of $\nabla^2\rho(r)$ are denoted by solid contours and positive values by dotted contours. In both cases the CBC plane is considered.

It is readily seen in Figure 4(a) that structure **1** is best described as a nearly T-shaped molecule rather than as a ring. There is no ring critical point, whereas the two B–C bond critical points collapse into a single bond critical point directed along the B–X line, X being the middle carbon–carbon point. Figure 4(b) confirms that electronic density is concentrated along the B–X line rather than along the B–C lines. A high concentration of density is also observed on the boron atom corresponding to the fully occupied 2*s* orbital. [When analysing Laplacian maps one should remember that negative values of $\nabla^2\rho(r)$, indicating concentration of charge density, are denoted by solid contours, whereas positive values reflecting depletion of charge density are represented by dotted contours. For example, the two shells of B and C atoms are easily visualized in those figures.]

Figure 5(a) clearly shows that there are no ring critical points but only C–C and B–X bond critical points for structure **2**. Nevertheless the interaction is very different from that in **1**. The values of the electron density (in a.u.) at the B–X bond critical point are 0.109 (structure **1**) and 0.008 (structure **2**). in fact Fig. 5(b) shows a closed-shell type interaction[49] for structure **2**, and no concentration of electron density between boron and the C_2 moiety. On the other hand, from Fig. 4(b) the interaction in **1** can be catalogued as a shared one.[49]

In the case of structure **3** it is readily seen in Fig. 6 that this is a truly three-membered ring. A ring critical point is found and the two B–C bond paths are slightly curved, giving a convex-shaped three-membered ring and suggesting that charge transfer takes place mainly from boron to the carbon atoms,[55] i.e. the b_2 interaction prevails over the a_1 interaction (the $3b_2$ molecular orbital is fully occupied in the $^2A_1$ state). Figure 6(b) clearly shows that electronic density is accumulated along the B–C lines, but there is also a large amount of charge density in the ring. In fact the charge density at the B–C bond critical points is 0.177 a.u., only slightly higher than the corresponding value at the ring critical point, namely 0.160. Therefore although the interactions between boron and ethylene in structures **1** and **3** are of the shared type, the bonding and charge density characteristics are quite different.

In the case of the BC_2H_2 system we have previously found[36] that the σ-complex between boron and acetylene can only be obtained at the Hartree–Fock (HF) level, whereas collapse occurs to the cyclic structure $BC_2H_2(^2A_1)$ when electron correlation effects are taken into account. A similar behaviour was observed in the

AlC_2H_4 system by Schaefer and co-workers.[19] They found that the σ-complex is an artifact of the HF method. Nevertheless we tried to obtain the boron–ethylene σ-complex and found the structure **4** shown in Fig. 7 at the MP2 level. However, its HF reference wavefunction is highly spin-contaminated ($\langle S^2\rangle = 1.067$) and consequently this result must be taken with caution. The electronic configuration of **4** is

$$(1a')^2(2a')^2(3a')^2(4a')^2(5a')^2(1a'')^2 (6a')^2(7a')^2(2a'')^2(8a')^2(9a')^1 \quad (9)$$

and it therefore correlates with the cyclic $^2A_1$ state (structure **3**). Furthermore, the unpaired electron is localized at the carbon atom non-bonded to boron. This fact, together with the bond distances shown in Fig. 7, suggests the valence-bond picture for **4** shown in Fig. 8. The $B–C_2$ distance is 2.362 Å and there is no overlap population between these two atoms.

We have also considered the $^2A''$ state resulting from $9a' \rightarrow 3a''$ promotion in electronic configuration (9), but this state, with the boron atom coplanar with the methylene group (Fig. 9), not only lies 2.9 (12.1) and 3.5 kcal mol^{-1} (14.6 kJ mol^{-1}) above **4** at the HF and PMP4 levels, respectively, but a vibrational analysis shows that in fact it is a transition state since it has an imaginary frequency corresponding to internal rotation. Therefore it was not considered further.

3.2 Boron–methylcarbene structures

Two different boron–methylcarbene structures have been found, corresponding to $^2A'$ and $^2A''$ electronic states (structures **5** and **6**, respectively, in Fig. 10). Both states are shown to be true minima since they have all frequencies real. The electronic configuration for the $2A'$ state is

$$(1a')^2(2a')(3a')^2(4a')^2(5a')^2(6a')^2 (1a'')^2(7a')^2(8a')^2(2a'')^2(9a')^1 \quad (9)$$

whereas the $^2A''$ state results from $2a'' \rightarrow 9a'$ promotion.

The geometrical parameters for structures **5** and **6**, especially the B–C bond distance, suggest quite a different bonding scheme in each case. Since the 2a″ molecular orbital in configuration (9) corresponds to a B–C π-type bonding, whereas in the case of the $^2A''$ state it is nearly a $2p$(C) orbital, the valence bond pictures shown in Fig. 11 may be proposed for structures **5** and **6**. These valence bond structures are confirmed by the atomic spin densities, which place the unpaired electron at boron (**5**) and at carbon (**6**), respecti-

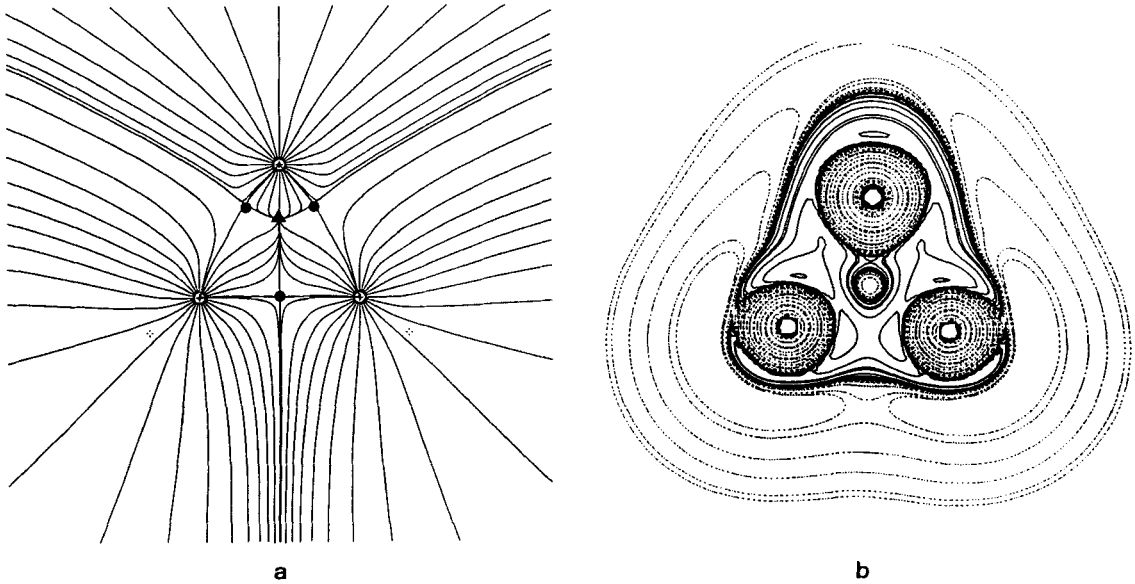

a b

Figure 6 (a) Gradient map of the electronic charge density and (b) contour map of the Laplacian of $\rho(r)$, for structure **3** obtained at the MP2/6-311G** level. In (a) the nuclei are denoted by crosses, bond critical points by dots and ring critical points by triangles. In (b) negative values of $\nabla^2\rho(r)$ are denoted by solid contours and positive values by dotted contours. In both cases the CBC plane is considered.

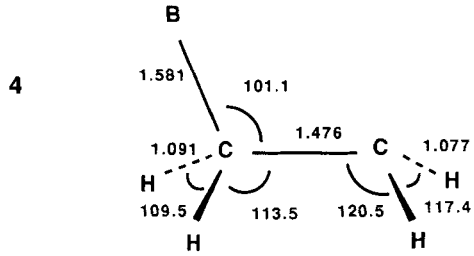

Figure 7 MP2/6-31G** optimized geometry for the σ-bonded boron–ethylene complex. Bond distances are given in Å and angles in degrees.

vely. In addition the B–C bond distance in **5** is coherent with a double bond.[57]

There is another possible conformer of the boron–methylcarbene system in which the unique hydrogen atom of the methyl group is in the *trans* position with respect to the boron atom. However, both the $^2A'$ and the $^2A''$ states of this structure are found to lie about 5 kcal mol^{-1} (21 kJ mol^{-1}) above the corresponding structures **5** and **6** at the MP4/6-311G** level. Furthermore, they have an imaginary frequency at the MP2/6-31G** level corresponding to the rotation of the methyl group.

3.3 Insertion products with a B–H bond

In the case of the BC_2H_2 system we found[36] that two of the candidates for the ground state are open and cyclic insertion products. In addition, although preliminary studies on the AlC_2H_4 system suggested the $^2B_2$ π-bonded isomer to be the lowest-lying isomer,[19] the same authors found that in fact the insertion product $HAlCHCH_2$ is the global minimum for AlC_2H_4.[58] Consequently it is of interest to explore the insertion products for the isovalent BC_2H_4 system.

The MP2/6-31G** optimized geometries for the open and cyclic insertion products (structures **7** and **8**, respectively) are shown in Fig. 12. In the case of structure **7** the *anti* isomer is found to lie slightly lower in energy than the *syn* conformation and therefore we will focus on the former. The

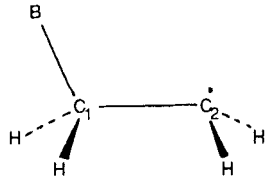

Figure 8 Valence bond structure of **4**.

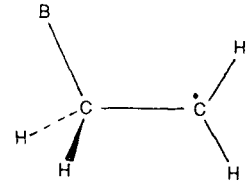

Figure 9 $^2A''$ valence bond structure, a transition state for internal rotation.

geometrical parameters (as well as the molecular orbitals) of structure **7** suggest the bonding scheme with a C–C double bond and the unpaired electron localized at the boron atom (Fig. 13). In fact the $^2A'$ state for the planar arrangement has an imaginary frequency associated with distortion of planarity due to the displacement of the hydrogen bonded to boron. Optimization under C_1 symmetry (instead of C_s) leads to a structure with a dihedral $\angle$HBCC angle of 161.3° at the MP2/6-31G** level. Nevertheless the potential surface is very flat for the variation of this angle. The non-polar structure lies only 0.5 kcal mol^{-1} (2.1 kJ mol^{-1}) below the planar *anti*-$HBCHCH_2$ species (with a dihedral angle of 180°) at the MP2/6-31G** level, whereas the other planar conformer (*syn*, with a dihedral angle of 0°) lies also just 0.6 kcal mol^{-1} (2.5 kJ mol^{-1}) above the non-planar structure at the same level of theory. However higher levels of theory suggest that it is quite likely that this isomer could indeed be planar, since at the PMP4 level the planar struc-

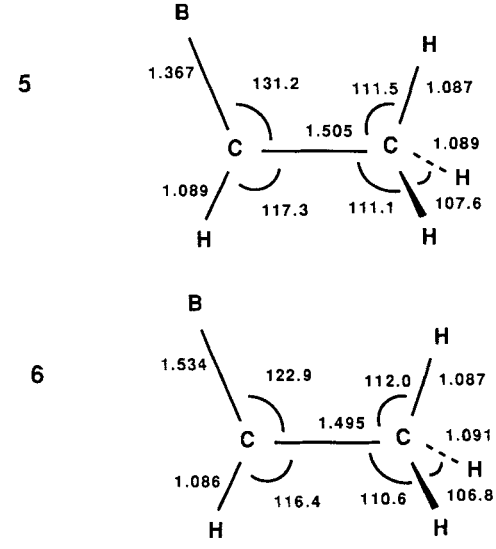

Figure 10 MP2/6-31G** optimized geometries for the boron–methylcarbene structures **5** and **6**. Bond distances are given in Å and angles in degrees.

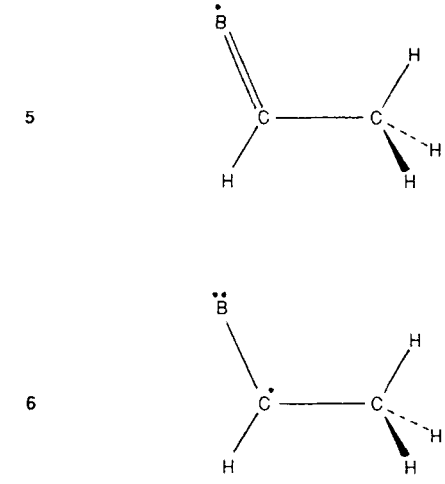

Figure 11 Valence bond structures of **7** and **8**.

ture (*anti*) lies slightly below the non-planar one. Therefore, although higher-level calculations are needed to establish a definitive conclusion about the planarity of this molecule, we have considered in what follows the $HBCHCH_2$ isomer in its planar *anti* conformation. The *syn* isomer (whose

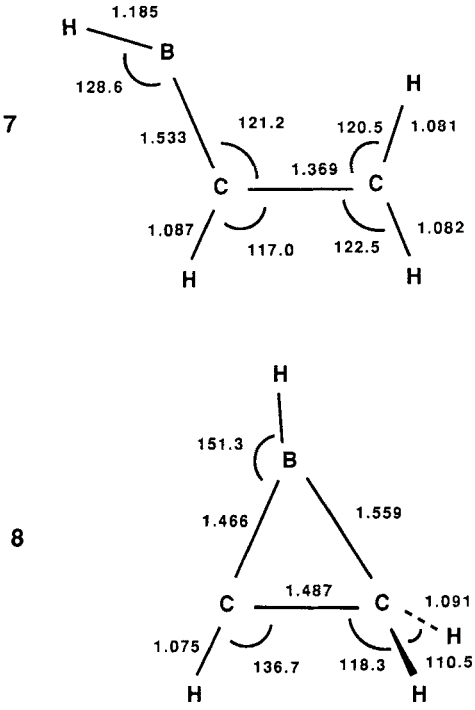

Figure 12 MP2/6-31G** optimized geometries for the $HBCHCH_2$ and HBC_2H_3 insertion products. Bond distances are given in Å and angles in degrees.

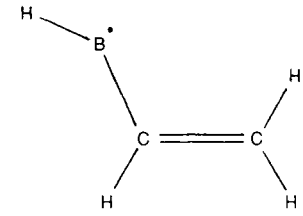

Figure 13 Valence bond structure of *anti*-**8**.

geometrical parameters resemble very much those of the *anti* isomer) lies only 0.3 kcal mol^{-1} (1.3 kJ mol^{-1}) higher than the *anti* conformation at the PMP4 level of theory. It is very likely then that conversion between both conformations can take place.

In the case of the cyclic insertion product, which corresponds to a $^2A''$ state, the hydrogen bonded to boron remains on the BCC plane, thus preserving the C_s symmetry. The unpaired electron is localized at the C_1 atom (the half-filled molecular oribtal is essentially a $2p_z(C_1)$ orbital) and the bond distances suggest the formation of a three-membered ring. This is confirmed by analysing the charge density. The gradient map of $\rho(r)$ and contour map of $\nabla^2\rho(r)$ for structure **8** are shown in Figs 14(a) and 14(b) respectively. In Figure 14(a) two B–C bond paths (slightly curved) and a ring critical point can be observed. Also, the contour map of $\nabla^2\rho(r)$ resembles very much (for the CBC unit) that found for structure **3** (Fig. 6b) which is also a three-membered ring. The values of $\rho(r)$ at the critical points are also very similar for **3** and **8**. For $B–C_1$ and $B–C_2$ bond critical points we find values of 0.188 and 0.170 a.u., respectively (0.177 a.u. for structure **3**), whereas the charge density is 0.165 a.u. at the ring critical point (0.160 a.u. for **3**).

3.4 Isomers with two B–H bonds

We have also searched for stable species with two boron–hydrogen bonds. It should be stressed that, for the reaction of boron with methane, CH_2BH and CH_2BH_2 are the major products detected in matrix isolation studies.[59]

The optimized geometries for H_2BCHCH (**9**) and H_2BCCH_2 (**10**) are shown in Fig. 15. Structure **9** corresponds to a $^2A'$ electronic state with the unpaired electron localized at the terminal carbon atom and a C–C double bond, as illustrated by the bond distances and angles. It has all frequencies real and distortion from the

planar geometry does not improve its energy, so planarity for this species is guaranteed.

In the case of the H_2BCCH_2 species, optimization without symmetry constraints leads to structure **10** with a BCC linear backbone, the hydrogen atoms of the CH_2 group on the same plane as the boron and carbon atoms, and the two hydrogens bonded to boron in the perpendicular plane. Structure **10** has therefore C_{2v} symmetry and corresponds to a $^2B_2$ electronic state with the following electronic configuration:

$$(1a_1)^2(2a_1)^2(3a_1)^2(4a_1)^2(5a_1)^2(6a_1)^2 (1b_2)^2(7a_1)^2(1b_1)^2(2b_1)^2(2b_2)^1 \quad (11)$$

The $2b_1$ orbital represents the C–C π-bond (made up from the $2p_x$ atomic orbitals) whereas the $2b_2$ molecular orbital is essentially the $2p_y$ orbital of central carbon, although it is highly delocalized towards boron, resulting in a B–C bond distance which is clearly shorter than that of a typical single bond. The charge transfer from central carbon to boron through delocalization of the $2b_2$ orbital amounts to $0.2\,e$. This favourable interaction between the $2p_y$ orbitals of central carbon and the boron atom, shown in Fig. 16, is the reason for the geometry of this species, with the HBH plane perpendicular to the CCH_2 moiety.

4 RELATIVE ENERGIES OF THE STABLE SPECIES

Table 1 shows the energies of the stable species relative to $B(^2P) + C_2H_4(^1A_g)$ at different levels of theory with the 6-311G** basis set on the MP2/6-31G** optimized geometries. We provide the HF, MP4 and projected MP4 (PMP4) results. In addition, we also give the PMP4 values (which should be the most reliable) corrected with scaled[60] zero-point vibrational energy differences. It is observed that there are no severe discrepancies between projected and non-projected MP4 values. The worst case is structure **4**, for which a difference of 4.7 kcal mol^{-1} (19.7 kJ mol^{-1}) is found between PMP4 and MP4 results; this is not surprising since its HF wavefunction is highly spin-contaminated, namely $\langle S^2\rangle = 1.067$. Spin contamination is also noticeable for structures **5**, **9** and **10** (with $\langle S^2\rangle$ values of 0.915, 0.930 and 0.841, respectively). All other structures have nearly spin-pure HF wavefunctions with $\langle S^2\rangle$ values smaller than 0.76. It is well known that the MP perturbation series converges slowly when spin contamination is high, but this shortcoming can be avoided quite efficiently employing spin-projected methods,[45,46,61,62], especially when spin contamination comes mainly from one single contaminant. In our case all the structures **4**, **5**, **9** and

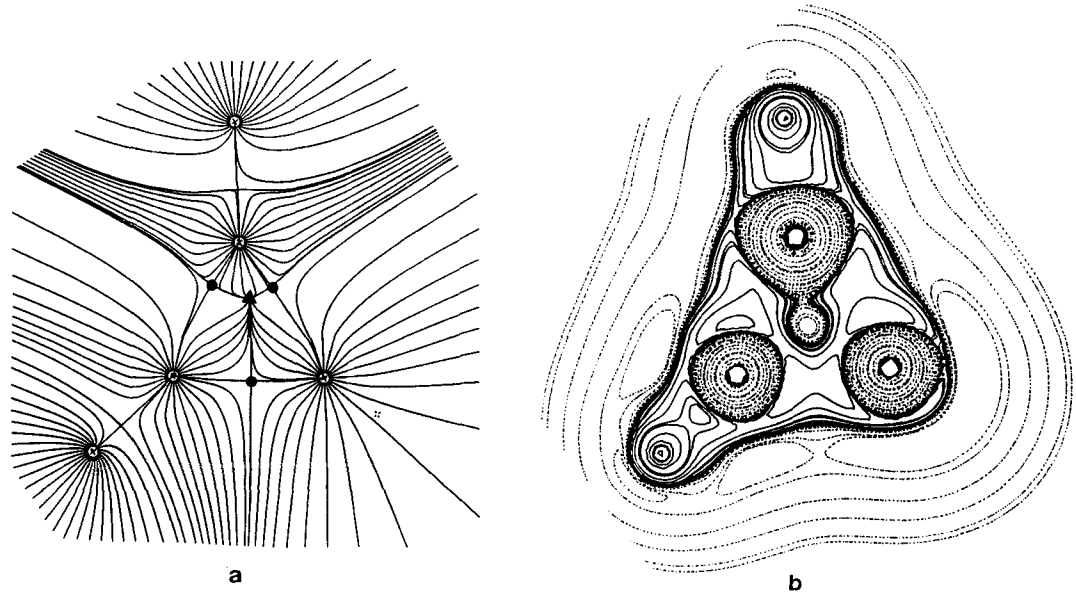

Figure 14 (a) Gradient map of the electronic charge density and (b) contour map of the Laplacian of $\rho(r)$, for structure **8** obtained at the MP2/6-311G** level. In (a) the nuclei are denoted by crosses, bond critical points by dots and ring critical points by triangles. In (b) negative values of $\nabla^2\rho(r)$ are denoted by solid contours and positive values by dotted contours. In both cases the CBC plane is considered.

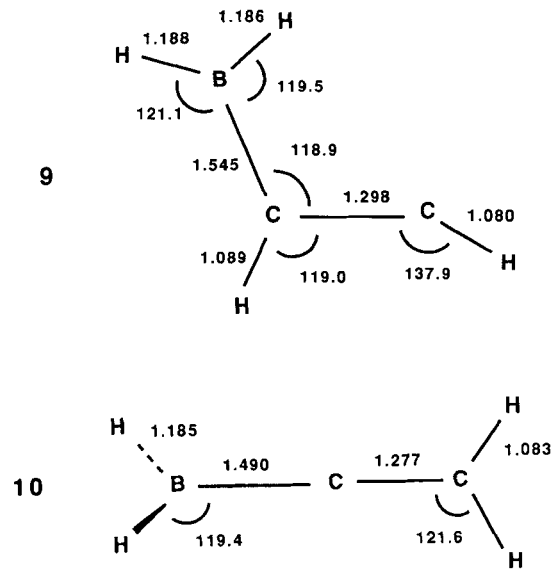

Figure 15 MP2/6-31G** optimized geometries for the H_2BCHCH and H_2BCCH_2 structures. Bond distances are given in Å and angles in degrees.

10 have S^2 expectation values very close to 0.75 after annihilation of the highest-spin contaminant, and therefore the projected MP values should be quite reliable. This is confirmed by our previous experience with similar systems. For example, in the case of the BC_2H_2 system we obtained[36] very similar results for the relative

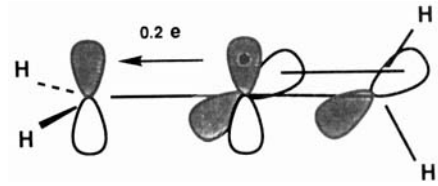

Figure 16 Interaction between the $2p_y$ orbitals of the central carbon and the boron atom in **10**.

energies of the three lowest-lying states at the projected MP level to Andrews *et al.*[29] employing (with a similar basis set) CCSD(T) theory (coupled cluster method with single and double excitations and perturbative inclusion of connected triple excitations), even if one of the species was highly spin-contaminated.

As can be seen in Table 1, all species are bonded relative to ground-state boron + ethylene. Nevertheless **2** (the long-distance π-complex) appears to be nearly isoenergetic with $B + C_2H_4$ at the HF level and only about 1 kcal mol^{-1} (4 kJ mol^{-1}) below at correlated levels. The $^2B_2$ state (structure **1**) is clearly more stable than **2**, as a result of the interactions qualitatively described in Section 3.1. However, the most stable C_{2v} cyclic structure by far is **3** [30 kcal mol^{-1} (13 kJ mol^{-1}) below **1**]. It is also interesting to note that **3** is also much more stable than the σ-complex (structure **4**).

Of the two boron–methylcarbene type structures, the more stable is **5**, which corresponds to a

Table 1 Relative energies (kcal mol^{-1})[a] of the stable species of the BC_2H_4 system with respect to $B(^2P) + C_2H_4(^1A_g)$, calculated at the HF, MP4 and PMP4 levels with the 6-311G** basis set on the MP2/6-31G** optimized geometries

Species	HF	MP4	PMP4	PMP4 + ΔZPVE[b]
1 $BC_2H_4(^2B_2)$	−4.5	−17.9	−18.1	−14.8
2 $BC_2H_4(^2B_1)$	0.0	−1.3	−1.6	−1.3
3 $BC_2H_4(^2A_1)$	−39.1	−46.3	−46.2	−44.6
4 $BC_2H_4(^2A')$	−20.3	−15.9	−20.6	−20.6
5 $BCHCH_3(^2A')$	−33.2	−33.3	−36.3	−34.2
6 $BCHCH_3(^2A'')$	−27.9	−28.1	−28.3	−26.9
7 $HBCHCH_2(^2A')$	−56.5	−59.4	−59.7	−58.9
8 $HBC_2H_3(^2A'')$	−47.8	−53.4	−53.7	−54.5
9 $H_2BCHCH(^2A')$	−55.3	−48.9	−52.9	−53.6
10 $H_2BCCH_2(^2B_2)$	−64.7	−63.8	−66.3	−66.6

[a] 1 kcal mol^{-1} = 4.184 kJ mol^{-1}.

[b] Zero-point vibrational energy differences were obtained by scaling the MP2/6-31G* vibrational frequencies.

$^2A'$ state and implies a double bond between boron and carbon. This is in contrast with what Xie *et al.*[19] reported for the isovalent AlC_2H_4 system. This discrepancy may be due to the reluctance of second-row atoms to form multiple bonds in comparison with their first-row counterparts.

The two insertion products with a B–H bond, **7** and **8**, are quite stable, the open structure **7** lying about 4 kcal mol^{-1} (16.7 kJ mol^{-1}) below the cyclic one. In fact, in the case of the AlC_2H_4 system Xie and Schaefer[58] found that the $HAlCHCH_2$ structure (the analogue of **7**) is the global minimum. However, no structures with two Al–H bonds are reported for the AlC_2H_4 system. In the case of BC_2H_4 these structures, **9** and **10**, are also quite stable, and furthermore the H_2BCCH_2 isomer is predicted to be the global minimum at all levels of theory, lying more than 8 kcal mol^{-1} (33.5 kJ mol^{-1}) below structure **7** at the PMP4 + ΔZPVE level. It is not surprising that structure **10** is so stable, since it has a C–C double bond as well as a certain degree of multiple bonding between boron and central carbon.

The main conclusion of the present work is therefore that the global minimum of BC_2H_4 is the H_2BCCH_2 isomer (structure **10**), but also that there are other species which are quite stable and might be accessible to experimental detection. Among these the more interesting are the open structures **7** and **9** lying about 8 (33.5) and 13 kcal mol^{-1} (54.4 kJ mol^{-1}) higher than H_2BCCH_2, and the cyclic structures **8** and **4**, which lie 12 (50.2) and 22 kcal mol^{-1} (92 kJ mol^{-1}), respectively, above the global minimum.

Acknowledgement This research has been supported by the Ministerio de Educación y Ciencia of Spain (DGICYT PB91-0207-C02-02).

REFERENCES

1. Z. Yuan, N. J. Taylor, R. Ramachandran and T. B. Marder, *Appl. Organomet. Chem.* **10**, 305–316 (1996).
2. W. H. Breckenridge and H. Unemoto, *Adv. Chem. Phys.* **50**, 325 (1982).
3. R. W. Zoellner and K. J. Klabunde, *Chem. Rev.* **84**, 545 (1984).
4. J. M. Parinis and G. A. Ozin, *J. Phys. Chem.* **93**, 1204 (1989).
5. P. H. Kasai, D. McLeod and T. Watanabe, *J. Am. Chem. Soc.* **99**, 3521 (1977).
6. P. H. Kasai, *J. Am. Chem. Soc.* **104**, 1165 (1982).
7. S. A. Mitchell, B. Simard, D. M. Rayner and P. A. Hackett, *J. Phys. Chem.* **92**, 1655 (1988).
8. P. H. Kasal and D. McLeod, *J. Am. Chem. Soc.* **97**, 5609 (1975).
9. J. A. Howard, B. Mile, J. S. Tse and H. Morris, *J. Chem. Soc., Faraday Trans. 1* **83**, 3701 (1987).
10. L. Manceron and L. Andrews, *J. Phys. Chem.* **93**, 2964 (1989).
11. R. Srinivas, D. Sulzie and H. Schwarz, *J. Am. Chem. Soc.* **112**, 8334 (1990).
12. J. H. B. Chenier, J. A. Howard and B. Mile, *J. Am. Chem. Soc.* **109**, 4109 (1987).
13. M. Trenary, M. E. Casida, B., R. Brooks and H. F. Schaefer, *J. Am. Chem. Soc.* **101**, 1638 (1979).
14. A. C. Scheiner and H. F. Schaefer, *J. Am. Chem. Soc.* **107**, 4451 (1985).
15. Y. Xie, B. F. Yates and H. F. Schaefer, *J. Am. Chem. Soc.* **112**, 517 (1990).
16. S. Sakai and K. Morokuma, *J. Phys. Chem.* **91**, 3661 (1987).
17. J. Miralles-Sabater, M. Merchán and J. Nebot-Gil, *Chem. Phys. Lett.* **142**, 136 (1987).
18. J. S. Tse, *J. Am. Chem. Soc.* **112**, 5060 (1990).
19. Y. Xie, B. F. Yates, Y. Yamaguchi and H. F. Schaefer, *J. Am. Chem. Soc.* **111**, 6163 (1989).
20. J. R. Flores and A. Largo, *Chem. Phys.* **140**, 19 (1990).
21. G. V. Chertihin, L. Andrews and P. R. Taylor, *J. Am. Chem. Soc.* **116**, 3513 (1994).
22. L. Andrews and T. R. Burkholder, *J. Phys. Chem.* **95**, 8554 (1991).
23. T. R. Burkholder and L. Andrews, *J. Chem. Phys.* **95**, 8697 (1991).
24. P. Hassanzadeh and L. Andrews, *J. Phys. Chem.* **96**, 9177 (1992).
25. P. Hassanzadeh and L. Andrews, *J. Phys. Chem.* **97**, 4910 (1993).
26. L. Andrews and T. R. Burkholder, *J. Phys. Chem.* **96**, 10195 (1992).
27. L. Andrews and T. R. Burkholder, *J. Phys. Chem.* **97**, 3500 (1993).
28. L. Andrews, P. Hassanzadeh, T. R. Burkholder and J. M. L. Martin, *J. Chem. Phys.* **98**, 922 (1993).
29. L. Andrews, P. Hassanzadeh, J. M. L. Martin and P. R. Taylor, *J. Phys. Chem.* **97**, 5839 (1993).
30. J. M. L. Martin, P. R. Taylor, P. Hassanzadeh and L. Andrews, *J. Am. Chem. Soc.* **115**, 2510 (1993).
31. L. B. Knight, J. O. Herlong, T. J. Kirk and C. A. Arrington, *J. Chem. Phys.* **96**, 5604 (1992).
32. L. B. Knight, D. W. Hill, T. J. Kirk and C. A. Carrington, *J. Phys. Chem.* **96**, 555 (1992).
33. Y. M. Hamrick, R. J. Van Zee, W. Weltner, W. J. Lauderdale, J. F. Stanton and R. J. Bartlett, *J. Phys. Chem.* **95**, 2840 (1991).
34. G. H. Jeong, R. Boucher and K. Klabunde, *J. Am. Chem. Soc.* **112**, 3332 (1990).
35. Y. Hannachi, P. Hassanzadeh and L. Andrews, *J. Phys. Chem.* **98**, 6950 (1994).
36. J. R. Flores and A. Largo, *J. Phys. Chem.* **96**, 3015 (1992).

37. K. Krogh-Jespersen, D. Cremer, J. D. Dill, J. A. Pople and P. v. R. Schleyer, *J. Am. Chem. Soc.* **103**, 2539 (1981).
38. J. J. Eisch, B. Shafii and A. L. Rheingold, *J. Am. Chem. Soc.* **109**, 2526 (1987).
39. J. J. Eisch, B. Shafii, J. D. Odom and A. L. Rheingold, *J. Am. Chem. Soc.* **112**, 1847 (1990).
40. P. C. Hariharan and J. A. Pople, *Theor. Chim. Acta* **28**, 213 (1973).
41. M. M. Franci, W. J. Pietro, W. J. Hehre, J. S. Binkley, M. S. Gordon, D. J. DeFrees and J. A. Pople, *J. Chem. Phys.* **77**, 3654 (1982).
42. J. A. Pople and R. Krishnan, *Int. J. Quantum Chem.* **14**, 91 (1978).
43. R. Krishnan, M. J. Frisch and J. A. Pople, *J. Chem. Phys.* **72**, 4244 (1980).
44. R. Krishnan, J. S. Binkley, R. Seeger and J. A. Pople, *J. Chem. Phys.* **72**, 650 (1980).
45. H. B. Schlegel, *J. Chem. Phys.* **84**, 4530 (1986).
46. H. B. Schlegel, *J. Phys. Chem.* **92**, 3075 (1988).
47. M. J. Frisch, G. W. Trucks, M. Head-Gordon, P. M. W. Gill, M. W. Wong, J. B. Foresman, B. G. Johnson, H. B. Schlegel, M. A. Robb, E. S. Replogle, R. Gomperts, J. L. Andres, K. Raghavachari, J. S. Binkley, C., Gonzalez, R. L. Martin , D. J. Fox, D. J. DeFrees, J. Baker, J. J. P. Stewart and J. A. Pople, *GAUSSIAN 92*, Gaussian Inc., Pittsburgh, 1992.
48. W. J. Hehre, L. Radom, P. v. R. Schleyer and J. A. Pople, Ab Initio *Molecular Orbital Theory*, Wiley, New York, 1986.
49. R. F. W. Bader, *Atoms in Molecules. A Quantum Theory*, Clarendon Press, Oxford, 1990.
50. F. W. Biegler-Konig, R. F. W. Bader and T. H. Tang, *J. Comput. Chem.* **27**, 1924 (1980).
51. M. J. S. Dewar, *Bull. Soc. Chim. Fr.* **18C**, 79 (1951).
52. J. Chatt and L. A. Duncanson, *J. Chem. Soc.* 2939 (1530).
53. R. Hoffmann, H. Fujimoto, J. R. Swenson and C. C. Wan, *J. Am. Chem. Soc.* **95**, 7644 (1973).
54. C. Liang and L. Allen, *J. Am. Chem. Soc.* **113**, 1878 (1991).
55. D. Cremer and E. Kraka, *J. Am. Chem. Soc.* **107**, 3800 (1985).
56. D. Cremer and E. Kraka, *J. Am. Chem. Soc.* **107**, 3811 (1985).
57. C. M. Cook and L. C. Allen, *Organometallics* **1**, 246 (1982).
58. Y. Xie and H. F. Schaefer, *J. Am. Chem. Soc.* **112**, 5393 (1990).
59. P. Hassanzadeh, Y. Hannachi and L. Andrews, *J. Phys. Chem.* **97**, 6418 (1993).
60. D. J. DeFrees and A. D. McLean, *J. Chem. Phys.* **82**, 333 (1985).
61. P. J. Knowles and N. C. Handy, *J. Chem. Phys.* **88**, 6991 (1988).
62. N. C. Handy, M.-D. Su, J. Coffin and R. D. Amos, *J. Chem. Phys.* **93**, 4123 (1990).